EJN European Journal of Neuroscience

FENS Federation of European Neuroscience Societies

European Journal of Neuroscience, Vol. 45, pp. 1078–1084, 2017 doi:10.1111/ejn.13548

MOLECULAR AND SYNAPTIC MECHANISMS

Unbalanced synaptic inputs underlying multi-peaked frequency selectivity in rat auditory cortex

Chang Zhou, Can Tao, Guangwei Zhang, Sumei Yan, Lijuan Wang, Yi Zhou and Ying Xiong
Department of Neurobiology, Chongqing Key Laboratory of Neurobiology, Third Military Medical University, 30 GaoTanyan Street, Chongqing 400038, China

Keywords: frequency selectivity, *in-vivo* patchclamp, level invariance, primary auditory cortex

Edited by Panayiota Poirazi
Received 31 October 2016, revised 13 February 2017, accepted 20 February 2017

Abstract

By measuring the frequency selectivity at different intensities in the primary auditory cortex of adult rats, we found that a small group of cortical neurons can exhibit relatively weak but robust selectivity at multiple frequencies that are different from the most preferred frequency. Both *in vivo* multi-unit recordings (26/93 recordings) and single-unit recordings (16/137 neurons) confirmed that the preferred frequencies are periodic and have an averaged bandwidth (BW) of 0.3–0.4 octaves, which leads to multi-peaked frequency selectivity. Interestingly, the averaged bandwidth of the ripple in the frequency response tuning curve was invariant with the sound intensity. An investigation of the synaptic currents *in vivo* also revealed similar multi-peaked frequency selectivity for both excitation and inhibition. While the excitatory and inhibitory inputs were relatively balanced for most frequencies, the ratio between excitation and inhibition at the peak and valley of each ripple was highly unbalanced. Since this multi-peaked frequency selectivity can be observed at the synaptic, single-cell, and population levels, our results reveal a potential mechanism underlying the multi-peaked pattern of frequency selectivity in the primary auditory cortex.

Introduction

At a given intensity, an auditory neuron will only respond to a limited range of frequencies, which is known as the receptive field of frequency or frequency response area (Evans, 1972). For most auditory neurons, only a specific frequency can evoke the strongest responses in the frequency response area at a given intensity, which is known as the best frequency (BF). Meanwhile, there are also auditory neurons that exhibit a preference for multiple frequencies, which have been widely observed in different species. In the primary auditory cortex of anesthetized cats, multiple response peaks in the frequency selectivity were identified many years ago (Abeles & Goldstein, 1970; Phillips & Irvine, 1981; Sutter & Schreiner, 1991; Sutter, 2000). The difference between the various peaks was between 1.5 and 2 octaves for both the MUA (multi-unit activity) and LFP (local field potential) responses (Sutter & Schreiner, 1991; Norena *et al.*, 2008). Similar observations were reported in the primary auditory cortex of awake marmosets, where the spiking responses to the characteristic frequency (CF) in the presence of its harmonics were enhanced over the response to the CF alone (Aitkin & Park, 1993; Kadia & Wang, 2003). In the core auditory fields (A1 and AAF) of awake ferrets, a small proportion (12%) of neurons shows frequency sensitivity with harmonic-like patterns (Kalluri *et al.*, 2008). These results suggested that auditory neurons with multi-peaked frequency selectivity could be a small yet ubiquitous population in the mammalian auditory cortex.

However, most of these studies are based on investigations of electrophysiological data obtained from extracellular recording, and very little is known about the intracellular mechanisms underlying the multi-peaked frequency selectivity (De Ribaupierre *et al.*, 1972). Previous studies have suggested that both the frequency and intensity tuning of neurons in the auditory cortex are largely dependent on the integration of different synaptic inputs. The feedforward inhibition can shape the tuning of excitation through the iceberg effect and even generate various types of tuning properties (Wu *et al.*, 2008; Hromadka & Zador, 2009). It remains unclear whether similar or distinct synaptic mechanisms play a role in multi-peaked frequency selectivity.

In this study, we investigated multi-peaked frequency selectivity in the primary auditory cortex of the adult rat. We found that some cortical neurons (16/137, 11.7%) exhibit multi-peaked frequency selectivity. Recording of synaptic inputs (EPSCs & IPSCs) using *in vivo* whole-cell patch clamp further showed that the multi-peaked frequency selectivity can also be observed in both excitatory and inhibitory synaptic currents. In addition, the interplay between excitatory and inhibitory inputs could also contribute to the multi-peaked frequency selectivity; the excitatory and inhibitory synaptic inputs were relatively unbalanced in amplitude at the peaks and valleys. With these results, we have demonstrated a potential synaptic mechanism that may contribute to a better understanding of the multi-peaked frequency selectivity in the rat primary auditory cortex.

Correspondence: Yi Zhou and Ying Xiong, as above.
E-mails: zhouyisjtu@gmail.com and xiongying2001@163.com

Materials and methods

Animal preparation and sound generation

All animal procedures were approved by the Animal Care and Use Committee of the Third Military Medical University. All experimental procedures were performed in accordance with the approved protocols. Surgeries and recordings were performed in an acoustic room with electromagnetic shielding (Shenyang Sound Booth Factory, China). Adult female Sprague-Dawley rats (1.5 months old, 150–200 g) were anesthetized by urethane (150 mg/100 g). The head of the animal was fixed in position using a customized apparatus, and a craniotomy was performed to expose the right auditory cortex. The body temperature of the animal was maintained at 37.5 °C with a customized heating pad with a feedback circuit. A total of 103 rats were used in this study. The number of animals used in this study is relatively high because the only recordings selected for statistical analysis were those that lasted longer than five repetitions (~5 min for each repetition).

A free-field magnetic speaker (MF1, TDT Inc., USA) was placed 1 cm away from the left ear of the animal. The right ear canal was filled with cotton. The sound was generated and calibrated by a high speed DAQ (PCI-6251, National Instruments, USA) using customized LabVIEW programs. More technical details can be found in our previous publications (Lou *et al.*, 2014). To exclude the possible influence of distorted sound generation during recording, the sound generation was calibrated before and after each recording session to ensure reliable sound delivery in this study. The maximal total harmonic distortion of generated pure tones was lower than 0.5%.

After the anatomical localization of the auditory cortex in the adult rat (3–7 mm to the bregma) and craniotomy, a tungsten electrode (2 MΩ, WPI) was inserted into the supragranular layer (layer 4, 400–600 μm below the pial surface) to measure the characteristic frequency (a frequency at which a neuron can respond to the lowest sound pressure level)) at the recording site. The primary auditory cortex was then localized based on the gradient of characteristic frequencies from 3 to 5 recording sites.

In vivo *extracellular multi-unit recording*

The extracellular multi-unit recording was performed using parylene-coated tungsten electrodes (0.1 MΩ, WPI Inc., USA). The electrode was inserted into the cortex vertically by a micromanipulator to reach a depth of 400–600 μm below the pial surface. The pure tones (25 ms pure tone plus 5 ms ramp before and after the sinusoid signal), which consisted of different frequencies (0.5–64 kHz, 0.1 octave step) and intensities (0–70 dB, 10 dB step), were delivered and repeated at least five times. The signals of the neural ensembles were amplified and recorded by a TDT System 3 (10 kHz sampling rate; 20 000× gain, TDT Inc., USA). The detection threshold for spike activity was set at three times the standard deviation above the baseline. Brainware (TDT Inc., USA) was used for online analysis, and MATLAB scripts were used for offline analysis.

In vivo *patch-clamp recording*

After mapping the auditory cortex (Guo *et al.*, 2012; Profant *et al.*, 2013), an *in vivo* patch-clamp recording was performed to collect single neuron responses from layer 4 of the primary auditory cortex. Cell-attached recording mode was used to obtain extracellular action potentials. Voltage-clamp recording mode was used to isolate and record excitatory and inhibitory synaptic currents by holding the membrane potential at −70 mV and 0 mV respectively (Wu *et al.*, 2006). For the cell-attached loose-patch recording, ACSF was used as the internal solution (in mM: 2.5 $NaHCO_3$, 2.5 KCl, 1.2 NaH_2PO_4, 124 NaCl, 2 $CaCl_2$, 1 $MgCl_2$ and 20 Glucose). For the voltage-clamp recording, a potassium-based solution was used (in mM: 0.3 GTP, 125 Cs-gluconate, 5 TEA-Cl, 4 MgATP, 10 HEPES, 2 CsCl, 10 phosphocreatine,1 EGTA and 1.5 QX-314, pH 7.2). The sound stimulation was the same as that used for the multi-unit recording. The neuronal responses were amplified and recorded by a patch-clamp amplifier (EPC-10, HEKA Gmbh, Germany). We completely compensated for the pipette capacitance (30–50 pF) was and compensated for 45–50% of the series resistance (20–50 MΩ) to reach an effective series resistance of 10–25 MΩ. The excitatory synaptic current was recorded by holding the membrane potential at −70 mV, which is the reversal potential for inhibitory ionotropic ligand-gated neurotransmitter receptors that flux Cl−. The inhibitory synaptic current was recorded by holding the membrane potential at 0 mV, which is the reversal potential for excitatory neurotransmitter receptors that flux Na+ and K+. The neuronal signals were low-pass filtered at 2.9 kHz and sampled at 10 kHz (Patch Master 10, HEKA Gmbh).

Data analysis and statistics

To minimize the influence of variation in neuronal responses, all analysis was based on data from experiments with at least five repetitions. The tone-evoked response (spikes or synaptic currents) was measured within a window of 10–50 ms from the onset of the stimuli. The frequency response tuning curve was first smoothed using Bayesian Adaptive Regression Splines (BARS) (Wallstrom *et al.*, 2008) to reduce the potential influence of response fluctuation caused by an occasional burst of spikes. After identification of the best frequency (BF), a nearby local minimum (in either a lower frequency zone or higher frequency zone) in the frequency response tuning curve was identified, which had to be at least 20% less than the peak amplitude at the BF. If another peak was found with at least a 20% increase in amplitude compared with the local minimum, a ripple in the frequency response tuning curve was identified. A MATLAB toolbox named "Peakfinder" was used for the automatic detection of potential peaks and valleys with a threshold set at 20% (Yoder, 2016). If one or more ripples were detected in the frequency response tuning curve measured at 70 dB, a neuron with "multi-peaked frequency selectivity" was identified. *T*-test or paired *t*-test were used when two groups had statistically equal variances. Kruskal–Wallis test was used for groups with different variances (McKight & Najab, 2010).

Synaptic conductance

Excitatory and inhibitory synaptic conductance were derived from the following previous reports (Zhou *et al.*, 2010, 2012):

$$I(t) = G_r(V_m(t) - E(r) + G_e(t)(V_m(t) - E_e) + G_i(t)(V_m(t) - E_i)$$

where $I(t)$ represents the amplitude of the synaptic current. G_r and E_r are the resting conductance and membrane potential respectively. V_m is the holding voltage. G_e and G_i are the excitatory and inhibitory conductance respectively. E_e (0 mV) and E_i (−70 mV) are the reversal potentials for excitatory and inhibitory ion channels respectively.

The F_e value was calculated as the ratio between the amplitude of excitatory conductance and the total amplitude of excitatory and inhibitory conductance at a given intensity and frequency, as previously described (Wehr & Zador, 2003).

$$F_e = \frac{G_e}{G_e + G_i}$$

Results

Multi-peaked frequency selectivity observed in the MUA

After the anatomical and functional mapping of the auditory cortex, a tungsten electrode was advanced into layer 4 of the primary auditory cortex (A1) in the right hemisphere (Fig. 1A, see Methods for details). Pure tones, which consisted of different frequencies and intensities (25 ms pure tone plus 5 ms ramp before and after the sinusoidal signal, 0.5–64 kHz, 0.1 octave step, 0–70 dB, 10 dB step), were delivered to the left ear to probe the tonal receptive field (TRF). We observed that besides the best frequency, which can evoke the strongest responses, some tuning curves of the frequency responses at relatively high intensities showed clear multi-peaked frequency selectivity (26 of 93 recordings). Figure 1B shows an example where a frequency response tuning curve measured at 30 dB above the threshold exhibited multiple frequency preferences other than the best frequency. The MUA recordings showed that the recording sites with multi-peaked patterns can have very different best frequencies (Fig. 1C, BF from 2 kHz to 32 kHz, measured at 30 dB above the threshold). It is worth noting that the peaks of the different neurons did not overlap at constant frequencies, which further suggested that the phenomenon of multiple frequency selectivity is unlikely to be caused by sound distortion.

Multi-peaked frequency selectivity observed in single-unit activity

To better understand the nature of multi-peaked frequency selectivity, we recorded spike responses from single neurons using *in vivo* loose-patch recording (see Methods for details). From the representative case shown in Fig. 2A, the multi-peaked pattern can be easily identified at a relatively high intensity (30 dB or more above the threshold). For example, the tuning curve of frequency selectivity at either 50 dB or 70 dB shows a clear multi-peaked pattern in frequency tuning (Fig. 2A). A total number of 137 neurons were recorded, and 16 showed clear multi-peaked selectivity in frequency tuning at 30 dB above the minimal threshold. From the representative case, we noticed that the number of peaks was higher at 70 dB than 50 dB. Similar results were obtained from 16 neurons ($P < 0.05$, paired t-test for 16 neurons, Fig. 2B). To determine the relationship between sound intensity and the number of non-BF preferred frequencies, we compared the number of non-BF preferred frequencies and the intensity of sound stimulation. We found that the number of peaks increased as intensity increased ($R^2 = 0.94979$, Slope = 1.2653, Fig. 2C). Because the bandwidth of the receptive field also expanded as intensity increased, a strong positive correlation was found between the bandwidth of the receptive field and the number of peaks ($R^2 = 0.8281$, Slope = 0.3305, Fig. 2D). The averaged bandwidth of each ripple was not significantly different between the measurements made at different intensities ($P = 0.324$, paired t-test for 16 neurons, Fig 2E). We made similar observations at additional intensities (40–70 dB, $n = 16$ neurons, $P = 0.616$, Kruskal–Wallis test, Fig. 2F). The histogram of the averaged bandwidth of the ripples shows a peak of approximately 0.3–0.4 octaves in distribution (Fig. 2G).

In addition to the averaged bandwidth of the ripples, we also investigated the distance between the individual ripples. Table 1 shows the distance (mean ± SD, in octaves) between the ripples from the single-unit recordings measured at 70 dB. The distance between nearby ripples was approximately 0.3 octaves, which is similar to that of the averaged bandwidth. Figure 2H shows the relationship between the relative location of the ripples and the best frequency and sound intensity. The locations of the ripples were relatively stable at all intensities, with the exception of some ripples that were far from the best frequency.

Both excitatory and inhibitory synaptic inputs show multi-peaked patterns in frequency tuning

The interplay between excitatory and inhibitory synaptic inputs could largely determine the spike responses in cortical neurons. To understand the synaptic currents underlying the multi-peaked pattern in the frequency selectivity, we directly recorded both excitatory and inhibitory synaptic inputs using *in vivo* whole-cell voltage-clamp recordings. In 63 whole-cell recordings, we identified 11

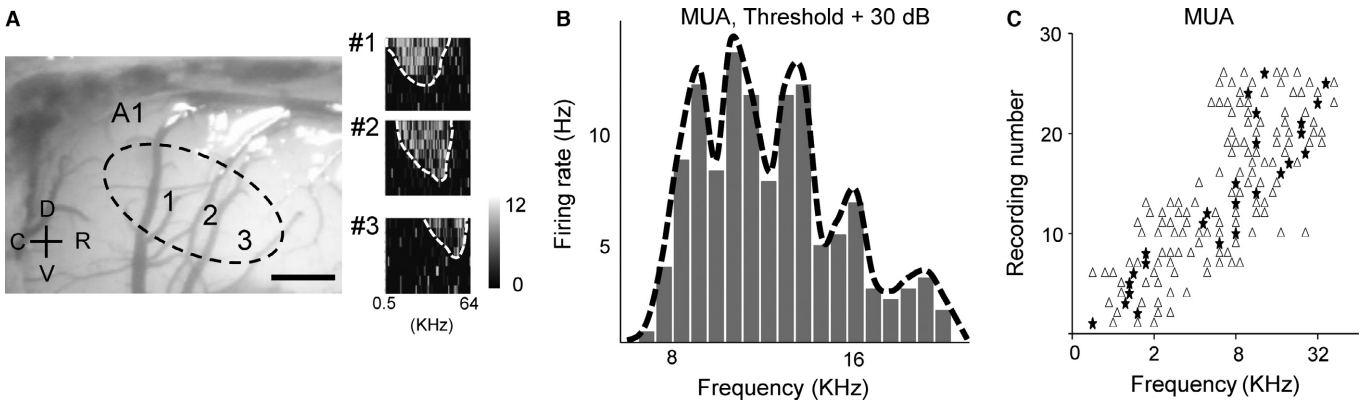

FIG. 1. Experimental design and multi-peaked frequency in MUA. (A) Mapping of primary auditory cortex. Different colors represent the firing rate (in Hz). Scale bar, 0.5 mm. (B) Example of multi-peaked frequency selectivity observed in MUA. Dashed line indicates the envelope of frequency tuning. (C) The multi-peaked frequency selectivity of MUA recorded from 26 recordings. Stars indicate the best frequency of each trial, and black triangles indicate preferred frequencies other than the best frequency.

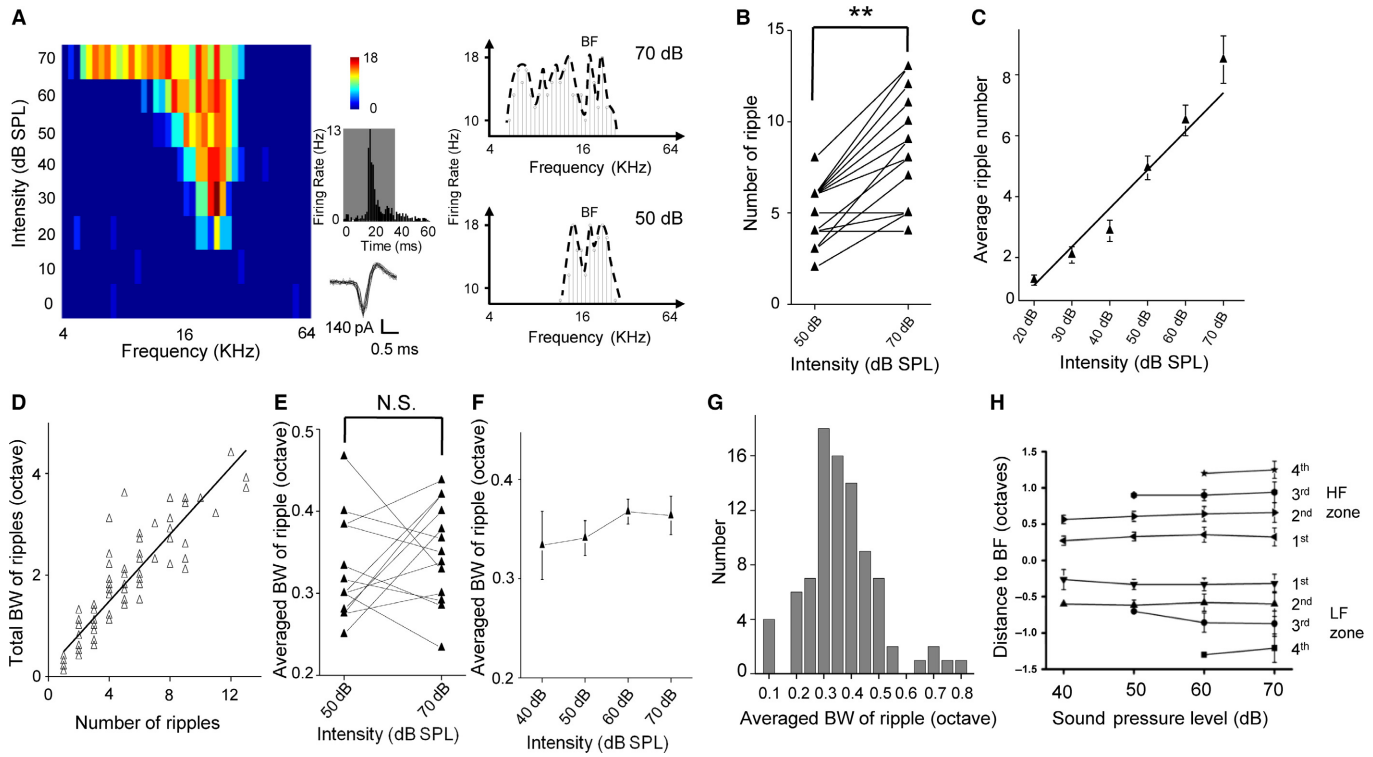

FIG. 2. Multi-peaked frequency selectivity in SUA. (A) Tonal receptive field of an example neuron. Different colors represent the firing rate (in Hz). Thirty superimposed spike waveforms and the peri-stimulus time histogram are shown on the right. Shaded area indicates the duration of the pure tone (25 ms pure tone plus 5 ms ramp before and after the sinusoid signal). Frequency response tuning curves measured at 50 dB and 70 dB are shown. Dashed lines indicate the smoothed envelopes of frequency selectivity. (B) Number of preferred frequencies measured at 50 dB and 70 dB from16 neurons. **, $P < 0.05$, paired t-test. (C) Relationship between sound intensity and the number of preferred frequencies (16 neurons, $R^2 = 0.9479$, slope = 1.2653. Error bar indicates SEM). (D) Relationship between the number of ripples and the total bandwidth of ripples (85 trials from 16 neurons, $R^2 = 0.8281$, slope = 0.3305). (E) Averaged bandwidth of the ripple at 50 dB and 70 dB from one example neuron. $P = 0.324$, paired t-test. (F) Averaged bandwidth of ripples measured at different intensities (64 trials from 16 neurons). (Error bar indicates SEM, $P = 0.616$, Kruskal–Wallis test). (G) Histogram of the averaged bandwidth of the ripples (85 trials from 16 neurons). (H) Location of the ripples measured by the relative distance to the best frequency (BF) from 40 dB to 70 dB. Ripples in the HF (higher frequency) zone have positive locations, and ripples in the LF (lower frequency) zone have negative locations. [Colour figure can be viewed at wileyonlinelibrary.com].

TABLE 1. Spacing between ripples from SUA measured at 70 dB (in octaves)

	BF	1st ripple (higher band)	2nd ripple (higher band)	3rd ripple (higher band)	4th ripple (higher band)
BF		0.33 ± 0.12 (n = 16)	0.66 ± 0.14 (n = 16)	0.94 ± 0.14 (n = 10)	1.25 ± 0.12 (n = 10)
1st ripple (lower band)	0.32 ± 0.13 (n = 16)	0.64 ± 0.21 (n = 16)	0.98 ± 0.21 (n = 16)	1.27 ± 0.21 (n = 10)	1.58 ± 0.19 (n = 10)
2nd ripple (lower band)	0.60 ± 0.17 (n = 15)	0.91 ± 0.24 (n = 15)	1.25 ± 0.22 (n = 15)	1.57 ± 0.22 (n = 10)	1.88 ± 0.20 (n = 10)
3rd ripple (lower band)	0.87 ± 0.18 (n = 13)	1.20 ± 0.24 (n = 13)	1.55 ± 0.21 (n = 13)	1.83 ± 0.21 (n = 9)	2.14 ± 0.20 (n = 9)
4th ripple (lower band)	1.21 ± 0.20 (n = 11)	1.55 ± 0.25 (n = 11)	1.91 ± 0.21 (n = 11)	2.24 ± 0.20 (n = 8)	2.53 ± 0.23 (n = 8)

neurons that showed multi-peaked frequency selectivity. Figure 3A shows an example of a tuning curve of frequency selectivity of the synaptic inputs recorded in A1 and measured at 30 dB above the threshold (Fig. 3A). For this representative case, it is clear that multi-peaked frequency selectivity can be found in the tuning curve of both excitatory and inhibitory synaptic inputs. Similar to the spike responses, the number of ripples found in the excitatory and inhibitory currents also increased as the intensity of sound stimulation grew ($P < 0.05$ for both excitatory and inhibitory, paired t-test, $n = 11$ neurons, Fig. 3B. $R^2 = 0.9924$, Slope = 1.3868 excitatory. $R^2 = 0.9199$, Slope = 1.4061 inhibitory, $n = 11$ neurons, Fig. 3C). For the ratio between the bandwidth and the number of peaks, no significant difference was found among the different intensities ($P = 0.921$ excitatory; $P = 0.537$ inhibitory, paired t-test, Fig. 3D. EPSC, $P = 0.815$; IPSC, $P = 0.416$, Kruskal–Wallis test, $n = 11$ neurons, Fig. 3E). A strong positive correlation was identified between the bandwidth and the number of peaks in both the excitatory ($R^2 = 0.7555$, Slope=0.3055) and inhibitory currents ($R^2 = 0.8724$, Slope = 0.3089, $n = 11$ neurons, Fig. 3F). A histogram of the averaged bandwidth of each ripple shows a peak of approximately 0.3–0.4 octaves in distribution for both excitation and inhibition (Fig. 3G) which is consistent with the results of the spike responses.

Similar to the analysis of the SUA, we also investigated the distance between the individual ripples in the frequency response tuning curves of both the EPSCs and IPSCs. Tables 2 and 3 show the distance (mean ± SD, in octaves) between the ripples from the EPSCs and IPSCs measured at 70 dB. The distance between nearby ripples was approximately 0.3 octaves for both the EPSCs and IPSCs. Figure 3H shows the relationship between the relative

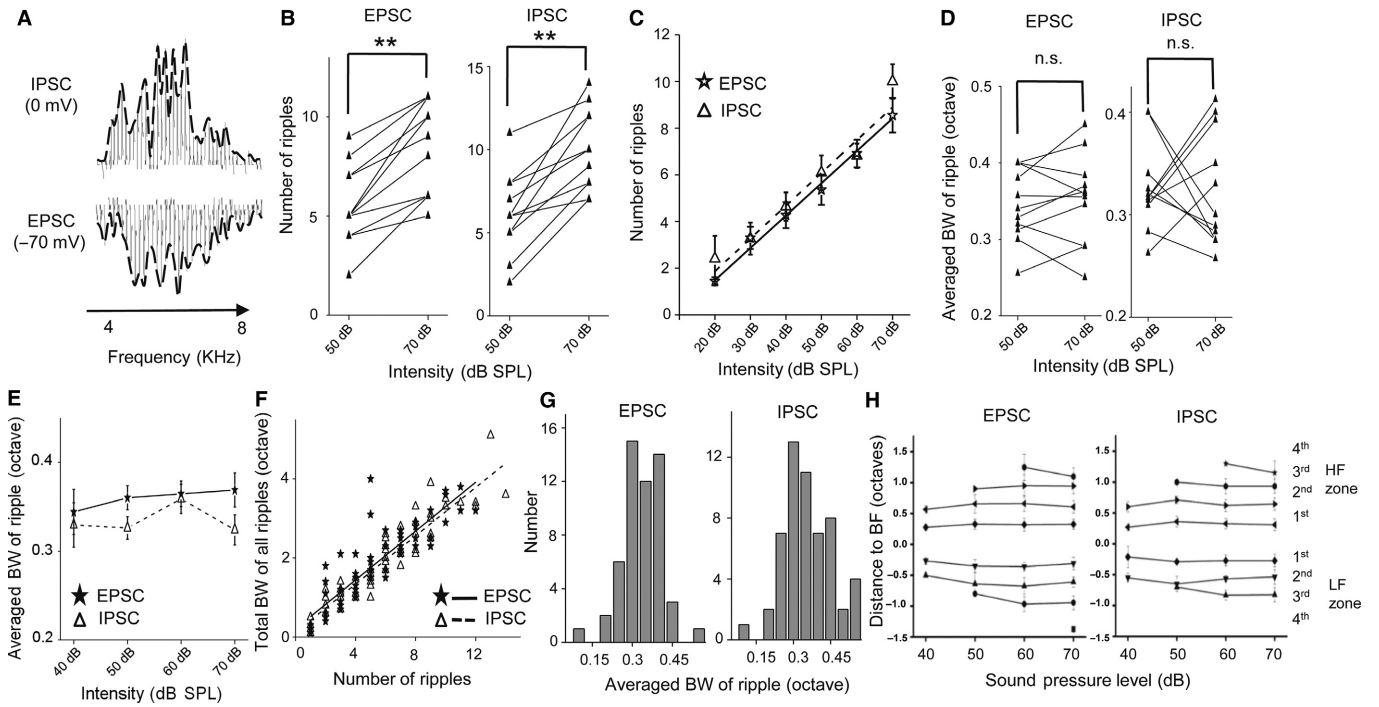

FIG. 3. Multi-peaked frequency selectivity of excitatory and inhibitory synaptic inputs. (A) Representative excitatory (solid line) and inhibitory (dashed line) inputs. (B) Number of preferred frequencies of the EPSCs and IPSCs measured at 50 dB and 70 dB from 11 neurons. **, $P < 0.05$ for both EPSC and IPSC, paired *t*-test. (C) Relationship between the sound intensity and the number of preferred frequencies of the synaptic inputs (11 neurons). EPSC, star and solid lines; IPSC, triangle and dashed lines, IPSC. Error bar indicates the SEM. EPSC, $R^2 = 0.9924$, slope = 1.3868; IPSC, $R^2 = 0.9199$, slope = 1.4061). (D) Averaged bandwidth of the ripples of the EPSCs and IPSCs measured at 50 dB and 70 dB from 11 neurons. EPSC, $P = 0.921$; IPSC, $P = 0.537$, paired *t*-test. (E) Relationship between the number of ripples and the total bandwidth of ripples (11 neurons, $R^2 = 0.8724$, slope = 0.3089). (F) Averaged bandwidth of the ripples of the EPSCs and IPSCs measured at different intensities (11 neurons, EPSC and IPSC respectively. EPSC, $P = 0.815$; IPSC, $P = 0.416$, Kruskal–Wallis test. The error bar indicates the SEM). (G) Histogram of the averaged bandwidth of each ripple measured from the EPSCs and IPSCs (11 neurons). (H) Location of the ripples measured by the relative distance to the best frequency (BF) from 40 dB to 70 dB. Ripples in the HF (higher frequency) zone have positive locations, and ripples in the LF (lower frequency) zone have negative locations.

TABLE 2. Spacing between ripples from EPSCs measured at 70 dB (in octaves)

	BF	1st ripple (higher band)	2nd ripple (higher band)	3rd ripple (higher band)	4th ripple (higher band)
BF		0.33 ± 0.08 (n = 11)	0.61 ± 0.10 (n = 11)	0.95 ± 0.12 (n = 11)	1.1 ± 0.14 (n = 2)
1st ripple (lower band)	0.31 ± 0.10 (n = 11)	0.64 ± 0.09 (n = 11)	0.92 ± 0.13 (n = 11)	1.25 ± 0.13 (n = 11)	1.45 ± 0.21 (n = 2)
2nd ripple (lower band)	0.61 ± 0.08 (n = 11)	0.94 ± 0.08 (n = 11)	1.22 ± 0.11 (n = 11)	1.55 ± 0.14 (n = 11)	1.6 (n = 1)
3rd ripple (lower band)	0.94 ± 0.11 (n = 9)	1.26 ± 0.11 (n = 9)	1.56 ± 0.14 (n = 9)	1.9 ± 0.16 (n = 9)	1.9 (n = 1)
4th ripple (lower band)	1.38 ± 0.05 (n = 4)	1.65 ± 0.06 (n = 4)	1.95 ± 0.13 (n = 4)	2.225 ± 0.13 (n = 4)	2.4 (n = 1)

location of ripples to best frequency and sound intensity from EPSCs and IPSCs. Similar to the observation in the SUA, the locations of the ripples were relatively stable at all intensities, with the exception of some ripples that were far away from the best frequency.

To better understand the contribution of the synaptic inputs to the multi-peaked frequency tuning of the spike responses, we further compared the averaged bandwidth of the ripples of the spike responses and synaptic inputs at different intensities (Fig. 4A, from 40 dB to 70 dB, $P = 0.674$, $n = 11$ neurons, Kruskal–Wallis test). The averaged bandwidths of the ripples in the frequency tuning between single neuron responses and synaptic inputs were not significantly different (Fig. 4B, N.S. means $P > 0.1$, Kruskal–Wallis test). Then, we explored the *E/I* ratio ("Fe" values, see Methods for details) in the whole receptive field to find potential explanations in the synaptic currents underlying the multi-peaked pattern (Wehr & Zador, 2003b). A large Fe value means relatively strong excitation with weak inhibition and vice versa. As shown in Fig. 4C, while the excitatory and inhibitory inputs were relatively balanced (324/405 stimuli of Fe values between 0.4 and 0.7, accounted for 80%), there was still a notable amount of unbalanced synaptic excitation and inhibition reflected by the extremely low or high Fe values (less than 0.4 or greater than 0.7, accounted for 20%). Figure 4D shows the Fe values measured at the peak and valley of each ripple based on the frequency selectivity of the EPSC, which is the major driving force in spike generation. The significant difference (82 peaks and 82 valleys, $P < 0.05$ paired *t*-test, Fig. 4D) between the Fe values suggested that unbalanced excitation or inhibition could further shape the multi-peaked frequency selectivity.

Discussion

Multi-peaked frequency selectivity in the MUA, SUA, and synaptic inputs

In this study, we reported the multi-peaked frequency selectivity in the rat primary auditory cortex, which was observed in both the

TABLE 3. Spacing between ripples from IPSCs measured at 70 dB (in octaves)

	BF	1st ripple (higher band)	2nd ripple (higher band)	3rd ripple (higher band)	4th ripple (higher band)
BF		0.31 ± 0.09 (n = 11)	0.64 ± 0.10 (n = 9)	0.93 ± 0.11 (n = 9)	1.15 ± 0.19 (n = 4)
1st ripple (lower band)	0.27 ± 0.10 (n = 11)	0.58 ± 0.15 (n = 11)	0.91 ± 0.15 (n = 9)	1.2 ± 0.17 (n = 9)	1.5 (n = 1)
2nd ripple (lower band)	0.54 ± 0.12 (n = 11)	0.85 ± 0.16 (n = 11)	1.18 ± 0.17 (n = 9)	1.47 ± 0.2 (n = 9)	1.7 (n = 1)
3rd ripple (lower band)	0.83 ± 0.12 (n = 8)	1.17 ± 0.10 (n = 6)	1.48 ± 0.13 (n = 5)	1.76 ± 0.18 (n = 5)	2 (n = 1)
4th ripple (lower band)	N/A	N/A	N/A	N/A	N/A

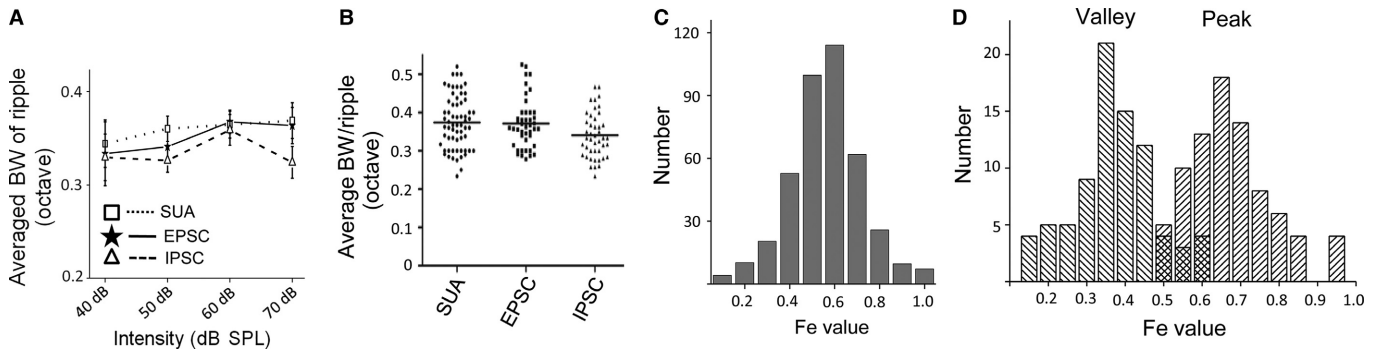

FIG. 4. *E*/*I* ratio underlying multi-peaked frequency selectivity. (A) Averaged bandwidth of the ripples of the SUA, EPSCs and IPSCs measured at different intensities (SUA, 16 neurons; EPSC and IPSC, 11 neurons, P = 0.674, Kruskal–Wallis test. Error bar indicates the SEM). (B) Comparison of the averaged bandwidth of the ripples among the SUA (64 ripples from 16 neurons), EPSCs (44 ripples from 11 neurons) and IPSCs (44 ripples from 11 neurons). (C) Histogram of Fe values measured from 11 neurons (405 stimuli in total). (D) Fe values measured at the valley and peak of each ripple (n = 82, valley and peak, respectively. $P < 0.05$, paired t-test).

SUA and MUA. Generally, the response patterns observed from single neuron activities could be different from those of the MUA due to the averaging of responses from different types of neurons (Gibson *et al.*, 2012; Keller *et al.*, 2016). Only robust and coherent patterns can be well-maintained in the activity of neuronal ensembles. Thus, the multi-peaked frequency selectivity could be a robust feature of cortical neurons in the processing of frequency information. Moreover, the averaged bandwidth of the ripple is consistent (0.3–0.4 octaves), which was found to be invariant with the sound intensity and the characteristic frequency of the recorded neuron (Figs 1 and 2). Although it remains unclear how this multi-peaked frequency selectivity can contribute to the coding of frequency information, researchers have suggested that neurons with multi-peaked frequency selectivity could be potentially involved in the processing of pitch-related sound cues (Kadia & Wang, 2003). It is worth noting that the spacing between nearby ripples is different from that of previous works, where 1.0–2.0 octaves were reported in cat and monkey, which could be a species-dependent difference (Sutter & Schreiner, 1991; Kadia & Wang, 2003; Norena *et al.*, 2008).

Although the averaged bandwidth is invariant with the sound intensity, we did observe a shift in the ripple locations as the sound intensity changed. If there is no shift in location, then we should be able to see clear ripples from the averaged responses across different intensities, which we did not. However, we found that it was difficult to measure the change in the ripple locations because we also noticed that as the sound intensity changed, the best frequency of many recorded neurons varied within a range of 0.1–0.2 octaves. Since the ripples are detected based on the best frequency at each intensity, and the distance between nearby ripples is approximately 0.3 octaves, a 0.1- to 0.2-octave variation in the best frequency makes it difficult to measure the change in the ripple locations at different intensities.

Synaptic contribution to the multi-peaked frequency selectivity

In the sensory cortex, the interplay between different synaptic inputs is critical for deciding the tuning properties of cortical neurons (Tan *et al.*, 2004). Tuning patterns could be relayed from presynaptic neurons (Zhou *et al.*, 2012) or created by spatially and temporally unbalanced excitation and inhibition (Tan *et al.*, 2007; Kuo & Wu, 2012). In this study, we found multi-peaked frequency selectivity in both the excitatory and inhibitory synaptic inputs, which suggested that it could be relayed from an earlier pathway, such as medial geniculate body (MGB). Because the response patterns observed in the auditory cortex could be the accumulated result of responses along the ascending pathway of the auditory system, it is difficult to determine the various contributions. Previous studies have shown that in some subcortical regions, such as the cochlear nucleus (VCN) in guinea pigs (Jiang *et al.*, 1996) and the lateral lemniscus in bats (Portfors & Wenstrup, 2001), there are neurons that show enhanced responses to multiple frequencies. These authors suggested that the multi-peaked frequency preference could originate from even earlier locations in the pathway than the MGB.

Although multi-peaked frequency selectivity was observed from both the SUA and synaptic inputs, it is difficult to interpret the relationship between the ripples generated by the synaptic inputs and the MUA/SUA responses because it is extremely difficult to record both activities from the same neuron in a living animal. One alternative method we used here is the measurement of the relationship between excitation and inhibition (*E*/*I* balance) at the peaks and valleys, which was represented by the Fe values. We found that the Fe values measured at the peaks are significantly higher than those measured at the valleys. This would make the firing at the peaks of the excitatory inputs even higher and the firing at the depths of the valleys even lower, which could further expand the response difference between the peaks and valleys. In other words, unbalanced

excitation and inhibition at the peaks and valleys could sharpen the ripples. It also worth noting that the averaged bandwidth of the ripples from the synaptic inputs is not significantly different from that of the spike responses, which suggests that the shaping is mainly dependent on the tuning sharpness rather than the bandwidth of ripple.

Acknowledgments

This work was supported by grants from the National Natural Science Foundation of China (No. 31371116 to YZ, No. 31271177, 31471056 to YX) and a grant from the 973 Young Scientist program (No. 2015CB759500 to YZ). We are grateful to the reviewers for very helpful comments on an earlier version of this manuscript.

Conflicts of interest

None.

Author contributions

YZ and YX designed the experiments and supervised the work. CZ, CT, GZ, SY, and LW performed the experiments. CZ and YZ wrote the manuscript. CZ prepared the figures.

Data accessibility

Supporting data and materials used in this study have been submitted to a data repository: https://doi.org/10.6084/m9.figshare.4641037.v1.

References

Abeles, M. & Goldstein Jr, M.H. (1970) Functional architecture in cat primary auditory cortex: columnar organization and organization according to depth. *J. Neurophysiol.*, **33**, 172–187.

Aitkin, L. & Park, V. (1993) Audition and the auditory pathway of a vocal New World primate, the common marmoset. *Prog. Neurobiol.*, **41**, 345–367.

De Ribaupierre, F., Goldstein Jr, M.H. & Yeni-Komshian, G. (1972) Intracellular study of the cat's primary auditory cortex. *Brain Res.*, **48**, 185–204.

Evans, E.F. (1972) The frequency response and other properties of single fibres in the guinea-pig cochlear nerve. *J. Physiol.*, **226**, 263–287.

Gibson, S., Judy, J.W. & Markovi, D. (2012) Spike sorting: the first step in decoding the brain: the first step in decoding the brain. *IEEE Signal Proc. Mag.*, **29**, 124–143.

Guo, W., Chambers, A.R., Darrow, K.N., Hancock, K.E., Shinn-Cunningham, B.G. & Polley, D.B. (2012) Robustness of cortical topography across fields, laminae, anesthetic states, and neurophysiological signal types. *J. Neurosci.*, **32**, 9159–9172.

Hromadka, T. & Zador, A.M. (2009) Representations in auditory cortex. *Curr. Opin. Neurobiol.*, **19**, 430–433.

Jiang, D., Palmer, A.R. & Winter, I.M. (1996) Frequency extent of two-tone facilitation in onset units in the ventral cochlear nucleus. *J. Neurophysiol.*, **75**, 380–395.

Kadia, S.C. & Wang, X. (2003) Spectral integration in A1 of awake primates: neurons with single- and multipeaked tuning characteristics. *J. Neurophysiol.*, **89**, 1603–1622.

Kalluri, S., Depireux, D.A. & Shamma, S.A. (2008) Perception and cortical neural coding of harmonic fusion in ferrets. *J. Acoust. Soc. Am.***123**, 2701–2716.

Keller, C.J., Chen, C., Lado, F.A. & Khodakhah, K. (2016) The limited utility of multiunit data in differentiating neuronal population activity. *PLoS One*, **11**, 1–20.

Kuo, R.I. & Wu, G.K. (2012) The generation of direction selectivity in the auditory system. *Neuron*, **73**, 1016–1027.

Lou, Y., Luo, W., Zhang, G., Tao, C., Chen, P., Zhou, Y. & Xiong, Y. (2014) Ventral tegmental area activation promotes firing precision and strength through circuit inhibition in the primary auditory cortex. *Front. Neural. Circuit.*, **8**, 25.

McKight, P.E. & Najab, J. (2010) *Kruskal-Wallis Test The Corsini Encyclopedia of Psychology*. John Wiley & Sons, Inc, Hoboken, NJ.

Norena, A.J., Gourevitch, B., Pienkowski, M., Shaw, G. & Eggermont, J.J. (2008) Increasing spectrotemporal sound density reveals an octave-based organization in cat primary auditory cortex. *J. Neurosci.*, **28**, 8885–8896.

Phillips, D.P. & Irvine, D.R. (1981) Responses of single neurons in physiologically defined primary auditory cortex (AI) of the cat: frequency tuning and responses to intensity. *J. Neurophysiol.*, **45**, 48–58.

Portfors, C.V. & Wenstrup, J.J. (2001) Responses to combinations of tones in the nuclei of the lateral lemniscus. *JARO*, **2**, 104–117.

Profant, O., Burianova, J. & Syka, J. (2013) The response properties of neurons in different fields of the auditory cortex in the rat. *Hearing Res.*, **296**, 51–59.

Sutter, M.L. (2000) Shapes and level tolerances of frequency tuning curves in primary auditory cortex: quantitative measures and population codes. *J. Neurophysiol.*, **84**, 1012–1025.

Sutter, M.L. & Schreiner, C.E. (1991) Physiology and topography of neurons with multipeaked tuning curves in cat primary auditory cortex. *J. Neurophysiol.*, **65**, 1207–1226.

Tan, A.Y.Y., Zhang, L.I., Merzenich, M.M. & Schreiner, C.E. (2004) Tone-evoked excitatory and inhibitory synaptic conductances of primary auditory cortex neurons. *J. Neurophysiol.*, **92**, 630–643.

Tan, A.Y., Atencio, C.A., Polley, D.B., Merzenich, M.M. & Schreiner, C.E. (2007) Unbalanced synaptic inhibition can create intensity-tuned auditory cortex neurons. *Neuroscience*, **146**, 449–462.

Wallstrom, G., Liebner, J. & Kass, R.E. (2008) An implementation of Bayesian adaptive regression splines (BARS) in C with S and R Wrappers. *J. Stat. Softw.*, **26**, 1–21.

Wehr, M. & Zador, A.M. (2003) Balanced inhibition underlies tuning and sharpens spike timing in auditory cortex. *Nature*, **426**, 442–446.

Wu, G.K., Li, P., Tao, H.W. & Zhang, L.I. (2006) Nonmonotonic synaptic excitation and imbalanced inhibition underlying cortical intensity tuning. *Neuron*, **52**, 705–715.

Wu, G.K., Arbuckle, R., Liu, B.H., Tao, H.W. & Zhang, L.I. (2008) Lateral sharpening of cortical frequency tuning by approximately balanced inhibition. *Neuron*, **58**, 132–143.

Yoder, N. (2016) Peakfinder – An Matlab toolbox that can quickly find local maxima (peaks) or minima (valleys) in a noisy signal.

Zhou, Y., Liu, B.H., Wu, G.K., Kim, Y.J., Xiao, Z., Tao, H.W. & Zhang, L.I. (2010) Preceding inhibition silences layer 6 neurons in auditory cortex. *Neuron*, **65**, 706–717.

Zhou, Y., Mesik, L., Sun, Y.J., Liang, F., Xiao, Z., Tao, H.W. & Zhang, L.I. (2012) Generation of spike latency tuning by thalamocortical circuits in auditory cortex. *J. Neurosci.*, **32**, 9969–9980.